Hypersherical Direction Cosine Transformation for Separation of Spectral and Illumination Information in Digital Scanner Data

Gregory W. Pouch and *David J. Campagna*
Department of Earth and Atmospheric Sciences, Purdue University, West Lafayette, IN 47907

ABSTRACT: Separation of topography-induced illumination effects and spectral information (cover type) in digital scanner data can be accomplished by projecting measurement vectors onto a hypersphere. The algorithm consists of calculating the radius R of the measurement vector $\mathbf{X}$ and its hyperspherical direction cosines $\mathbf{Y}$ for each measurement vector $\mathbf{R} = \left[\sum_i^{\text{bands}} X_i^2\right]^{1/2}$ and $\mathbf{Y} = \frac{\mathbf{X}}{\mathbf{R}}$. Machine classification of the data is greatly enhanced because spectral information (cover type) dominates the variance in the transformed data, while topography-induced illumination effects dominate original, untransformed data. This also offers significant improvements in visual analysis and possible advantages in multitemporal analysis.

INTRODUCTION

DATA GATHERED by digital scanner systems, such as the Landsat MSS and TM, and SPOT systems, contains two fundamental types of information: illumination and surface material reflectance. The brightnesses seen by a sensor are the product of the incident illumination (a constant factor for a given surface element) and the spectrum of the ground cover. Haze (and sensor bias) add a constant to the measurement vector, while sensor noise adds a random value. This relationship can be expressed mathematically as

$$\begin{bmatrix} X_1 \\ X_2 \\ \cdot \\ \cdot \\ \cdot \\ X_i \end{bmatrix} = \mathrm{SSG} \begin{bmatrix} S_1\, \tau_{11}\, R_{1p}\, \tau_{12} \\ S_2\, \tau_{21}\, R_{2p}\, \tau_{22} \\ \cdot \\ \cdot \\ \cdot \\ S_i\, \tau_{i1}\, R_{ip}\, \tau_{i2} \end{bmatrix} + \begin{bmatrix} H_1 \\ H_2 \\ \cdot \\ \cdot \\ \cdot \\ H_i \end{bmatrix} + \begin{bmatrix} N_1 \\ N_2 \\ \cdot \\ \cdot \\ \cdot \\ N_i \end{bmatrix} \quad (1)$$

where X is the measurement vector of a data set with i bands, p is the cover type of the pixel, SSG is a sun-slope geometry term accounting for illumination, R_{ip} is the reflectance of cover type p in a particular band i, S_i is the intensity of the irradiating sunlight, τ_{i1} and τ_{i2} are the atmospheric transmission factors for the inbound and outbound paths respectively, H_i is the haze level (and sensor bias), and N_i is the sensor noise. Note that the illumination term SSG is the same for all reflected bands for a given pixel, while only the reflective term R_{ip} depends on cover type.

It has been shown that the variance of a data set due to topographic expression is much greater than the variance due to the spectral response (Gillespie *et al.*, 1986). This has led to the development of techniques which enhance the spectral response of the data set. Generally, these techniques include (1) band ratioing (Rowan *et al.*, 1974; Podwysocki *et al.*, 1983; & Gillespie *et al.*, 1987), (2) directed band ratioing (Crippen *et al.*, 1988), and (3) decorrelation and saturation stretching (Gillespie *et al.*, 1986). Notably, these enhancement techniques have been developed with the visual interpretation of the data set in mind. Hence, the latter two techniques tend to enhance the spectral variation and retain the topographically derived variance within the data set.

In digital analysis of a sensor image, such as statistical classification based on spectral characteristics, it is often essential to separate the topographically induced variations in illumination from the spectral variations due to various cover types (an example of the effects of not separating topography from spectral information in the image can be seen in the clustering results shown in Plate 2e, where the clusters correspond to combinations of slope-aspect and cover type). Band ratioing, once the data have been properly adjusted for haze and sensor bias offset, removes the topographic expression (Crippen *et al.*, 1988). However, there are several problems associated with band ratioing for digital analysis. First is the loss of band significance in the final band ratio due to the division process itself. (For example, a high value for TM6/TM5 does not indicate whether it is due to strong reflectance in TM6 or strong absorption in TM5.) Second, the topographic information is not recoverable. Third, band ratios tend to saturate quite easily, because band ratios can range from 0 to infinity (or 255 if 1 is added to the denominator). Finally, and perhaps most significantly, the images that result from band ratioing seem to be noisier than the original data.

There is a need for a data transformation that separates the topographic expression and retains the band significance of the spectral reflectance. A hyperspherical direction cosine (HSDC) transformation satisfies this need. We examine the conceptual background of hyperspherical coordinates with respect to real data structure, present a simple algebraic procedure which implements the transform, and offer examples of the transformation on two different sensor datasets of two different regions.

THEORETICAL CONCEPTS

Viewing the data structure is helpful in understanding the effects of topography and spectral reflectance; for simplicity, two-dimensional bispectral plots are utilized. A spectrally homogeneous cover type will plot as a line segment radial to the origin as shown in Figure 1a. Because the relationship between spectral bands of the ideal cover type is constant, it is the slope of the line that identifies the cover type. The radial translation

0099-1112/90/5604–475$02.25/0

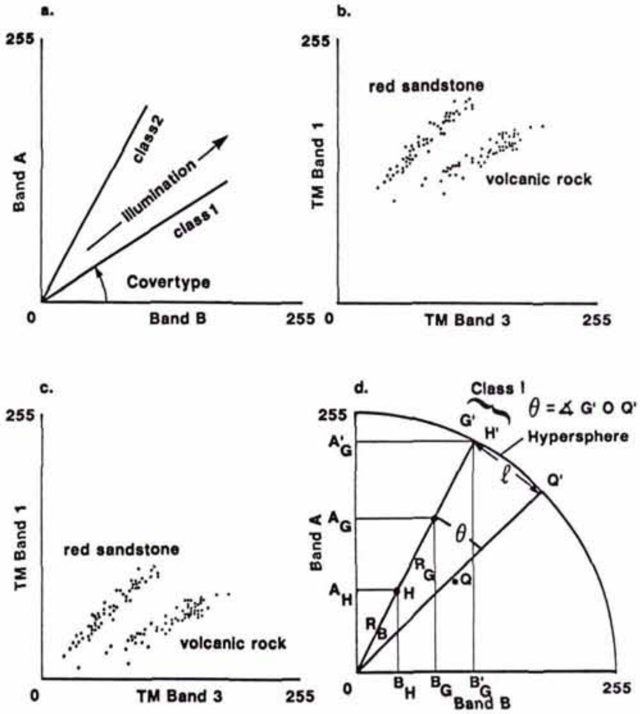

FIG. 1. Bispectral Plots. (a) Theoretical plot of two different spectrally-homogeneous classes. (b) Plot of two actual lithologic classes from the Landsat TM dataset. (c) Plot of same classes after haze adjustment. (d) Projection of three points (G, H, and Q) onto a hypersphere of radius 255 for two band data. G and H, which have the same reflectances but different radiances, plot at the same point (G' and H') on the hypersphere. Distance from a measurement vector to a class mean is angle Θ; an equivalent measure of distance would be the cartesian distance l between the vectors' projections on the hypersphere.

of a point along the line is due to variation in illumination caused by topography (the sun-slope geometry). In actual data, the cover classes exhibit a less precise form. As can be seen in Figure 1b, two cover classes sampled from actual data are represented by elliptical patches (rather than straight lines) whose long axes do not intersect at the origin. The scatter pattern is caused by lack of complete uniformity within the cover type as well as atmospheric and sensor noise. The offset of the axes relative to the origin is caused by atmospheric effects (notably "haze") and sensor bias. This offset can be adjusted by various methods so that the cover types are again radial to the origin, approximating the ideal situation. All the data presented in this article have been adjusted using the regression intersection method (Crippen, 1987) as shown in Figure 1c.

A common objective of digital image processing is to produce a class map from the sensor data. This mapping can be performed using supervised classification (ancillary data are used to statistically characterize user-defined classes; an example would be a maximum-likelihood classifer, which relies on training field selection) or unsupervised clustering (modes in the multi-dimensional data distribution are sought which define natural structure in the data; an example would be a moving means clustering program like ISODATA)

Most clustering criteria, such as maximizing the cluster-means distance while minimizing the cluster radius (which is equivalent to minimizing the sum square error (Swain and Davis, 1978)), use Pythagorean distance from cluster means to classify data points. Because Pythagorean distance shows no directional preference, the resulting clusters are hyperspheres and clustering is thus particularly vulnerable to sun-slope geometry effects. Judicious training field selection in supervised classification can mitigate this problem under favorable circumstances.

As seen in Figure 1d, angular proximity (θ in Figure 1d) of a measurement vector to a line is a better measure of class type than is proximity to a point. The best way to establish this proximity (nearness criterion) is to express the measurement vector of a pixel as an angular measure in hyperspherical coordinates. The radius is a measure of the illumination of the pixel and is effectively separated from the spectral reflectance measure. The implementation of this coordinate transformation is a very simple two-step process.

PROCEDURE

In hyperspherical coordinates, distance could be defined as the angular separation between two points, or the arccosine of their dot product. However, the Cartesian distance between two points on a hypersphere is an adequate surrogate for their angular distance as illustrated in Figure 1d. Because the hyperspherical direction cosines (the Cartesian components of a unit vector through the data point) are simpler and faster to compute than the angular position, and the hyperspherical direction cosines can be clustered or classified with standard algorithms designed for cartesian measurement vectors, we chose to implement hyperspherical direction cosines rather than hyperspherical angles. To transform a measurement vector into hyperspherical direction cosines, the radius measure is first calculated as

$$R = \left[\sum_{i}^{\text{bands}} X_i^2 \right]^{1/2} \tag{2}$$

where X_i is the pixel's brightness value in the ith band. The direction cosines are defined by

$$\begin{bmatrix} Y_1 \\ Y_2 \\ \cdot \\ \cdot \\ \cdot \\ Y_i \end{bmatrix} = \frac{255}{R} \begin{bmatrix} X_1 \\ X_2 \\ \cdot \\ \cdot \\ \cdot \\ X_i \end{bmatrix} \tag{3}$$

where Y_i is the direction cosine measure of the original measurement vector X_i. Because most remote sensing systems use an 8-bit integer for storage, the constant 255 is included in Equation 3. The operation described above is equivalent to radially projecting each measurement vector onto a hypersphere with a radius of 255. (A hypersphere is the n-dimensional equivalent of a sphere or circle and can be mathematically defined as the locus of all points $\mathbf{X}$, such that $|\mathbf{X}-\mathbf{C}|=r$, where C is the center of the hypersphere and r is its radius.)

TWO EXAMPLES OF THE HSDC TRANSFORMATION

To test the hyperspherical direction cosines transform, two data sets were used: the first, MSS data of a vegetated mountainous area; and the second, TM data of an arid mountainous area of exposed rock. The transformation's ability to enhance the discrimination of vegetation and lithology was shown as well as its ability to mitigate illumination effects on classification.

Prior to performing the transformation, the data sets were adjusted for haze and sensor bias as described previously. The HSDC transformation was applied to both data sets on an IBM-AT using the ERDAS program ALGEBRA. The original datasets and the transformed datasets (excluding the radial measure) were classified with an ERDAS-compatible moving-means clustering algorithm (written by G. Pouch, copyright 1989 by the

Purdue Research Foundation; contact the author for availability) using a number of classes for each area determined from the groundtruth class maps.

For the Santa Rita area (Plate 1), Richardson *et al.* (1979) stated that there are four distinct vegetation associations controlled by elevation and soil development. The original MSS dataset was collected in February, 1973 over the Santa Rita Mountains south of Tucson, Arizona, and a subscene of 150 by 150 pixels extracted from the original data set is shown as Plate 1a. A general elevation map constructed for use as the groundtruth map with which the resulting cluster classification maps are to be compared is shown as Plate 1b. The lowest elevations, shown in red and blue in Plate 1b, support a shrub-dominated plant community; the foothills and low mountains, shown in green, are forested; and the highest elevations, shown in orange and bright red, are above the treeline and also have a shrub-dominated plant community.

Plate 1c is the radius band for the Santa Rita MSS, whereas Plate 1d shows the hyperspherical direction cosines for MSS7, MSS5, and MSS4. Plates 1e and 1f show the clustering results based on the original data and the HSDC transformed data (exclusive of radius) for the Santa Rita Mountains. Visual examination of the cluster map of the original data (Plate 1e) shows strong illumination effects in the clustering. In particular, note that the shadowed areas in the mountains (western half of subscene) are classified into a separate class (dark green). In contrast, the clustering based on the HSDC data showed no such effect.

The TM dataset was collected in April, 1984 over the Lake Mead area of southern Nevada. Plate 2a is a subscene of 150 by 150 pixels extracted over Pinto Ridge, a simple anticlinal structure faulted along its northwestern boundary. The area is arid and nearly devoid of vegetation. Plate 2b is a class map based on field mapping; the geologic units were grouped into telegeologic units of similar spectral character based on laboratory spectra of hand samples. (Laboratory spectra were obtained with a Barnes radiometer with channels equivalent to TM.) In plate 2b, cherty limestone is blue, limestone-gypsum is green, redbeds are light red, volcanics (andesite) are intense red, alluvium with volcanic fragments is yellow-brown, and all other materials are shown in brown. In the clustering, two extra classes were added to account for the possibility of unsampled units (e.g., soils).

Plates 2e and 2f show the classification results for the Pinto Ridge area using both the original and transformed datasets, respectively. Inspection of the TM image of Pinto Ridge (Plate 2a) and the clustering of the original TM data (Plate 2e) shows that the latter is strongly affected by slope. Notice that the brightly-lit patches near the southeast limb of the anticline in the limestone-gypsum unit and the southeastern area of redbeds near the alluvial fan are both clustered together using the original data (blue in Plate 2e), but that no such effect is present in the HSDC-transformed clustering results. A similar effect can be seen for the dimly-lit portions of the above areas where shadowed areas were clustered together (shown in black in Plate 2e) in the original data whereas they show no particular pattern in the transformed image. Table 1 shows the number of points in each cluster in each lithologic class for the clustering of the original TM data, whereas Table 2 shows these values for the HSDC transformed clustering. While not as striking as the visual presentation of the data, Table 1 shows that clustering of the original data results in lithologic classes splitting into several similarly-sized clusters which contain several different lithologies, especially redbeds, limestone, limestone-gypsum, and volcanics, all of which tend to form rugged topography. In contrast, Table 2 shows that clustering of the HSDC transformed data results in the lithologic classes occupying fewer clusters and the clusters tending to be dominated by one or two lithologies.

Consideration of the clusterings based on the original data (Plates 1e and 2e) shows that they exhibit better correlations to the radius bands (Plates 1c and 2c) of the transformed images than to the class maps. On the other hand, the classification maps of the hyperspherical direction cosines (Plates 1f and 2f) show a strong correlation to the previously defined class maps and thus are controlled more by cover type than by sun-slope geometry.

DISCUSSION

As developed in the preceding theoretical arguments and demonstrated in the applied examples, the HSDC transform is successful in separating the variations in illumination due to topography from the spectral reflectance measure. Because albedo is defined as band independent reflectance (Swain and Davis, 1978), it is logically equivalent to illumination. Thus, albedo is aliased into the radius band and is not separated from the illumination.

The significant advantages of the separation of the two basic information types are numerous, and a few are mentioned below. As was shown, the HSDC transform allows more accurate separation of spectral classes using unsupervised statistical classification. Because numerical algorithms are sensitive to the numerical variance, the use of computationally simpler and faster supervised classification algorithms, such as a parallelepiped classifier, may be possible alternatives to the more commonly used and time consuming maximum-likelihood algorithms.

The hyperspherical direction cosines in a transformed image retain the band significance of the original measurement vector. To illustrate this, an arbitrary pixel was selected from the TM subset, and the digital numbers from the original and transformed data sets are compared in Figure 2. Retaining band significance allows a spectral interpretation of image color and should decrease illumination effects in commonly utilized transformations such as the tasseled cap or the normalized vegetation difference.

Another aspect of the transformation is the ability to reduce differences in multitemporal images arising from differences in the sun's position. The HSDC transform estimates the incident illumination from the remote sensing dataset, thus correcting for varying illumination without the use of ancillary datasets such as digital elevation models. The sun angle effects will simply be stored as the radial measure in the HSDC transformation.

The topographic expression is also an important data source in interpretation. The HSDC transformation retains this information in a separate band which is available for various analyses (e.g., drainage, landform).

The traditional band ratio method is equivalent to finding a direction tangent in a series of projection planes, while the HSDC transform finds the direction cosines in n-space. Because the cosine's derivative is bounded by 1 and -1, while the tangent has an unbounded derivative, we believe the HSDC is more stable in the presence of noise.

It may be noted that, because an accurate estimate of the scene illumination allows separation of spectral information, the addition of a panchromatic brightness band, with consequent very high signal-to-noise ratio, would be a useful addition to future digital scanners.

Finally, the implementation of the transform is extremely simple and fast. The only major preparation step is obtaining a reasonably accurate estimate of the numerical offset due to haze and sensor bias.

SUMMARY

The hyperspherical direction cosine transform successfully separates topography-controlled illumination effects and cover-controlled spectral effects in digital scanner data by projecting

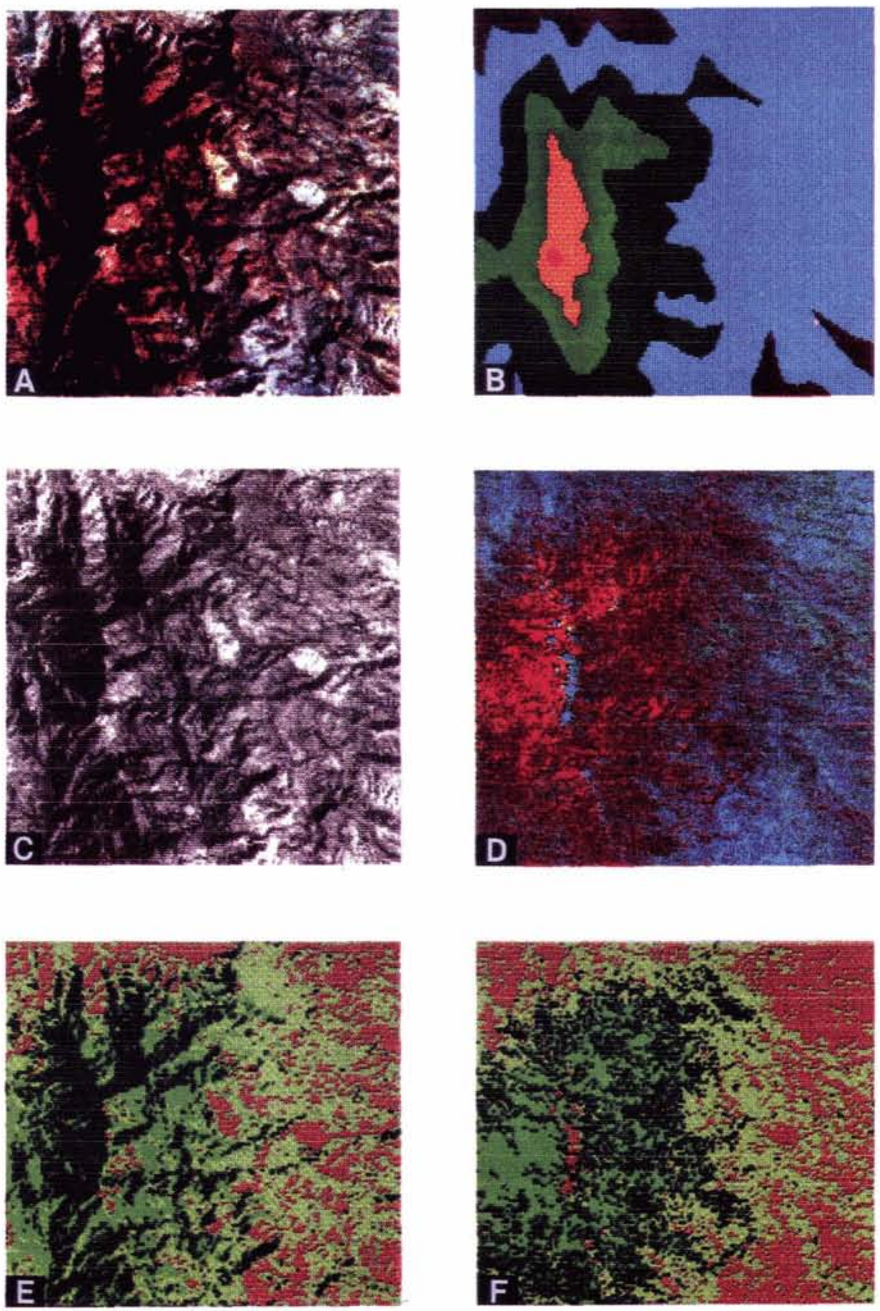

PLATE 1. Santa Rita Mountains, Arizona. (A) Landsat MSS (R = 7, G = 5, B = 4) false color image. (B) Elevation class map, 305 metre (1000 ft) color intervals. (C) Radius image. (D) Hyperspherical Direction Cosines (R = 7, G = 5, B = 4) false color image. (E) ISODATA classification results of original dataset. Note shadowing effects in class assignments. (F) ISODATA classification results of HSDC data set.

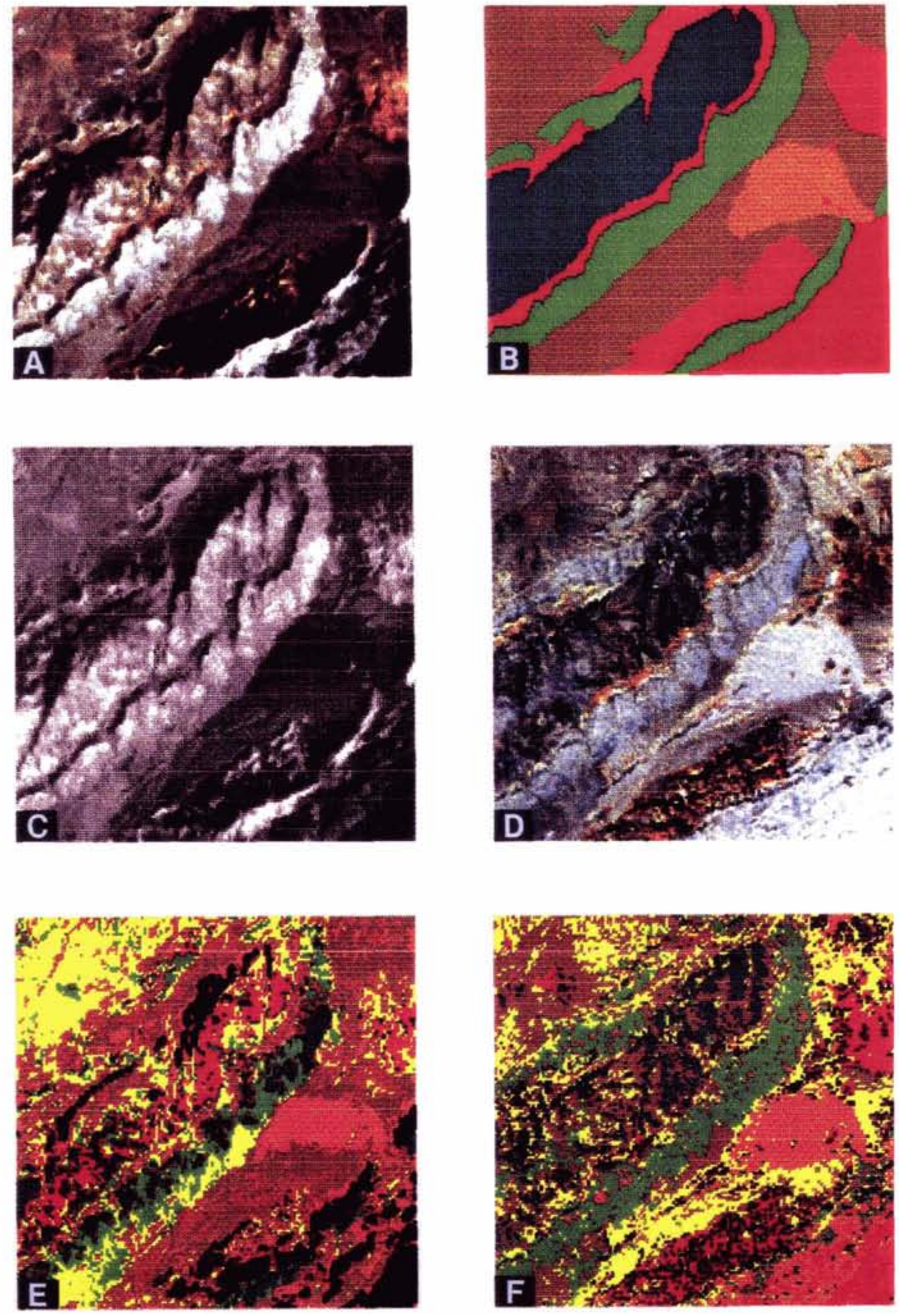

PLATE 2. Pinto Ridge, Nevada. (A) Landsat TM (R = 3, G = 2, B = 1) color image. (B) Telegeologic spectral units. (C) Radius image. (D) Hyperspherical Direction Cosine (R = 3, G = 2, B = 1) color image. (E) ISODATA classification of original image. Note shadows and brightly-lit slopes in original image. (F) ISODATA classification results of Hyperspherical Direction Cosine dataset.

TABLE 1. CLASSIFICATION RESULTS FOR ORIGINAL TM DATA
ENTRIES REPRESENT THE NUMBER OF PIXELS BELONGING TO THE CLUSTER SPECIFIED BY COLUMN AND THE LITHOLOGY SPECIFIED BY ROW. NOTE THE TENDENCY OF LITHOLOGIC CLASSES TO BREAK INTO SEVERAL SIMILARLY SIZED CLASSES, ESPECIALLY THE VOLCANICS, LIMESTONES, AND REDBEDS, WHICH ARE RIDGE-FORMERS, AND OF CLUSTERS TO CONTAIN SEVERAL LITHOLOGIES. REFER TO PLATES 2B AND 2E FOR VISUAL COMPARISON.

	Cluster Number								
Lithology	1	2	3	4	5	6	7	8	Lithology Total
QAL	615	2559	21	1900	48	411	1980	116	7650
Redbeds	177	575	48	749	310	519	800	384	3562
Limestone and Gypsum	1284	501	855	278	344	256	360	209	4087
Cherty Limestone	425	699	446	322	1287	304	414	289	4186
Andesite Volcanics	52	33	25	351	3	609	155	625	1853
Alluvial Fan	0	5	0	352	0	783	22	0	1162
Cluster Totals	2553	4372	1395	3952	1992	2882	3731	1623	22500

TABLE 2. CLUSTERING RESULTS FOR HSDC-TRANSFORMED TM DATA OF PINTO RIDGE
ENTRIES REPRESENT THE NUMBER OF PIXELS BELONGING TO THE CLUSTER SPECIFIED BY COLUMN AND THE LITHOLOGY SPECIFIED BY ROW. NOTE THE TENDENCY FOR LITHOLOGIC CLASSES TO OCCUPY RELATIVELY FEWER CLUSTERS, AND THE TENDENCY FOR CLUSTERS TO CONTAIN ONLY ONE OR TWO LITHOLOGIES. REFER TO PLATES 2B AND 2F FOR VISUAL COMPARISON.

	Cluster								
Lithology	1	2	3	4	5	6	7	8	Lithology Total
QAL	2789	639	501	2620	525	6	179	391	7650
Redbeds	636	256	66	783	444	19	358	1000	3562
Limestone and Gypsum	394	2258	487	644	106	20	142	36	4087
Cherty Limestone	490	305	37	1885	27	0	1426	16	4186
Andesite Volcanics	44	152	829	82	2	680	64	0	1853
Alluvial Fan	122	16	934	17	56	0	6	11	1162
Cluster Totals	4475	3626	2854	6031	1160	725	2175	1454	22500

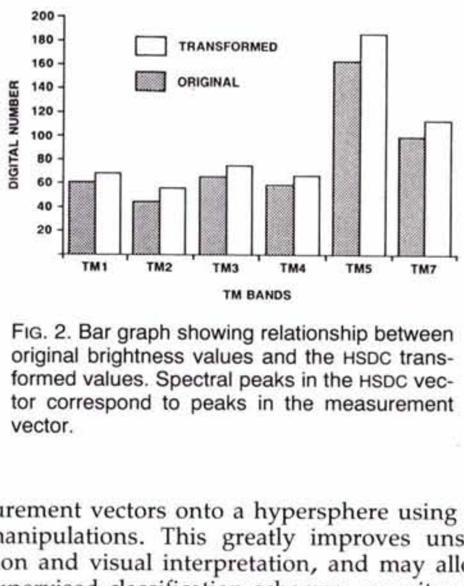

FIG. 2. Bar graph showing relationship between original brightness values and the HSDC transformed values. Spectral peaks in the HSDC vector correspond to peaks in the measurement vector.

the measurement vectors onto a hypersphere using simple algebraic manipulations. This greatly improves unsupervised classification and visual interpretation, and may allow use of simpler supervised classification schemes, permit easier registration of multitemporal data, and reduce illumination effects in other band transformations.

ACKNOWLEDGMENTS

We wish to thank Barringer Geoservices for the TM data of Pinto Ridge and Purdue University LARS for the MSS data of the Santa Rita Mountains. We thank our advisor Dr. D.W. Levandowski for encouragement and support and Larry Biehl of Purdue's Electrical Engineering Department for assistance with laboratory spectra. G. Pouch was supported in part by the Indiana Mining and Mineral Resources Research Institute.

REFERENCES

Crippen, R.E., 1987. The regression intersection method of adjusting image data for band ratioing. *International Journal of Remote Sensing*, 8, 137–155.

Crippen, R.E., R.G. Blom, and J.R. Heyada. 1988. Directed band ratioing for the retention of perceptually-independent topographic expression in chromaticity-enhanced imagery. *International Journal of Remote Sensing*, 9, 749–765.

Gillespie, A.R., A.B. Kahle, and R.E. Walker, 1986. Color enhancement of highly correlated images. I. Decorrelation and HSI contrast stretches. *Remote Sensing of the Environment*, 20, 209–235.

———, 1987. Color enhancement of highly correlated images II: Channel ratio and "chromaticity" transformation techniques. *Remote Sensing of the Environment*, 22, 343–365.

Podwysocki, M.H., D.B. Segal, and M.J. Abrams, 1983. Use of multispectral scanner images for assessment of hydrothermal alteration in Marysvale, Utah, mining area. *Economic Geology*, 78, 675–687.

Richardson, M.L., S.D. Clemmons, and J.C. Walker, 1979. *Soil Survey of Santa Cruz and Parts of Cochise and Pima Counties, Arizona*, USDA Soil Conservation Service, Washington, D.C.

Rowan, L.C., P.H. Wetlaufer, A.F.H. Goetz, F.C. Billingsley, and J.H. Stewart, 1974. *Discrimination of Hydrothermally Altered Areas of Rock Types Using Computer Enhanced ERTS Images, South Central Nevada.* USGS Professional Paper 883.

Swain, P.H., and S.M. Davis (eds.), 1978. *Remote Sensing: The Quantitative Approach*, New York, McGraw-Hill.

Erratum

In the article, "A System for Digital Stereo Image Matching," by Marsha Jo Hannah, which appeared on pages 1765-1770 of the December issue of *PE&RS*, the photographs for Figures 3 through 5 were installed in the wrong order, i.e., the caption for Figure 3 is accompanied by the photo intended for Figure 5, the caption for Figure 4 was paired with photo 3, and the caption for Figure 5 is with photo 4.